

# Atom Probe Tomography Investigation of Lath Boundary Segregation and Precipitation in a Maraging Stainless Steel

M. Thuvander,\* M. Andersson,\*\* K. Stiller\*

\* Department of Applied Physics, Chalmers University of Technology, SE-412 96 Göteborg, Sweden

\*\* R&D Centre, Sandvik Materials Technology, SE-811 81 Sandviken, Sweden

## Abstract

Lath boundaries in a maraging stainless steel of composition 13Cr-8Ni-2Mo-2Cu-1Ti-0.7Al-0.3Mn-0.2Si-0.03C (at.%) have been investigated using atom probe tomography following aging at 475°C for up to 100 h. Segregation of Mo, Si and P to the lath boundaries was observed already after 5 min of aging, and the amount of segregation increases with aging time. At lath boundaries also precipitation of  $\eta$ -Ni<sub>3</sub>(Ti, Al) and Cu-rich 9R, in contact with each other, takes place. These co-precipitates grow with time and because of coarsening the area number density decreases. After 100 h of aging a ~5 nm thick film-like precipitation of a Mo-rich phase was observed at the lath boundaries. From the composition of the film it is suggested that the phase in question is the quasicrystalline R' phase. The film is perforated with Cu-rich 9R and  $\eta$ -Ni<sub>3</sub>(Ti, Al) co-precipitates. Not all precipitate types present in the matrix do precipitate at the lath boundaries; the Si-containing G phase and  $\gamma'$ -Ni<sub>3</sub>(Ti, Al, Si) and the Cr-rich  $\alpha'$  phase were not observed at the lath boundaries.

Keywords: atom probe tomography; stainless steel; maraging steel; lath boundaries; precipitation; segregation

## 1. Introduction

Martensitic precipitation hardening (PH) stainless steels are characterized by high strength and toughness obtained through addition of alloying elements like Cr, Ni, Cu, Mo, Ti and Al that, after an optimized heat treatment, result in formation of nanosized and densely distributed intermetallic precipitates. The precipitates act as effective obstacles for dislocation movements, which explains the good mechanical properties of the steels. Atom probe tomography (APT) has been a key technique governing the understanding of the precipitation processes of PH stainless steels [1-5].

During the 1990's, a martensitic PH stainless steel called Nanoflex<sup>®</sup> was developed by Sandvik Materials Technology. The strength of this steel ultimately reaches 3000 MPa, while it sustains high ductility and fracture toughness [6, 7]. Aging at 475°C results in a gradual increase in strength for aging times as long as 1000 h [6], which is in contrast to most other PH steels. The unusually high strength was previously ascribed to the occurrence of the quasicrystalline Mo-rich R' phase [6, 7]. However, detailed studies (mostly by atom probe techniques) of the development of the steel microstructure during aging revealed a much more complex reality in which several precipitating phases are involved [5, 8, 9]. It has been shown that after 5 min of aging, there is a high number density of Cu/Ni/Ti/Al/Si-rich clusters. These clusters develop within 4 h of aging into multiphase particles, consisting of either Cu-rich 9R and  $\gamma'$ -Ni<sub>3</sub>(Ti, Al, Si) precipitates or Cu-rich 9R and  $\eta$ -Ni<sub>3</sub>(Ti, Al) precipitates. After this stage of aging, Cr-rich  $\alpha'$  phase nucleates in contact with the multiphase particles. Finally, within 100 h of aging, there is a phase transformation of  $\gamma'$ -Ni<sub>3</sub>(Ti, Al, Si) into G-Ni<sub>16</sub>Si<sub>7</sub>Ti<sub>6</sub> phase [8, 9] and Mo-rich quasicrystalline R' precipitates are formed in contact with the multiphase particles. The precipitation process in the martensitic matrix can thus be summarized as follows:

Cu-rich clusters + Ni/Ti/Al/Si-rich clusters (5 min) →

9R +  $\eta$ -Ni<sub>3</sub>(Ti, Al) +  $\gamma'$ -Ni<sub>3</sub>(Ti, Al, Si) (4 h) →

9R +  $\eta$ -Ni<sub>3</sub>(Ti, Al) +  $\gamma'$ -Ni<sub>3</sub>(Ti, Al, Si) +  $\alpha'$  (40 h) →

9R +  $\eta$ -Ni<sub>3</sub>(Ti, Al) + G-Ni<sub>16</sub>Si<sub>7</sub>Ti<sub>6</sub> +  $\alpha'$  + R' (100 h)

Although the phase separation routes in the martensitic matrix of the steel are at present quite well understood, the grain and lath boundary chemistry and its development are less well documented. This is despite the fact that due to the dense distribution of these interfaces they probably influence the mechanical properties of the material. It is a well recognized fact that grain and lath boundaries can be treated as weak links in the structure, due to a relatively weak binding between the atoms and because of possible segregation of impurity elements (like P, Sn, Sb, etc.), which in many cases reduce the boundary cohesion and deteriorate the mechanical properties of steels. Furthermore, due to the faster diffusion of alloying elements at the lath boundaries, the precipitated phases normally grow faster at these locations, which may also influence the mechanical properties of the material. Here we report about an APT study of the evolution of the lath boundary microstructure in Nanoflex during aging at 475°C.

## 2. Experimental Procedures

The steel Nanoflex<sup>®</sup> investigated in the present work was produced and provided by Sandvik Materials Technology. Its chemical composition (at.% and balanced with iron) was 13.0 Cr, 8.5 Ni, 2.3 Mo, 1.7 Cu, 1.1 Ti, 0.69 Al, 0.30 Mn, 0.24 Si and 0.03 C. The material was solution treated at 1050°C and water quenched. The volume fraction of martensite was maximized by cold rolling the material into strips (deformation degree of 83%) that resulted in deformation-

induced martensite. In the subsequent aging procedure the material was aged for 5 min, 4 h, 40 h and 100 h at 475°C.

Two versions of LEAP [10] instruments from Imago Scientific Instruments were used; a 3000X Si and an energy compensated (reflectron) 3000X HR with improved mass resolution. The LEAP 3000X Si was used for the analyses of material aged for 4 h and 40 h. The LEAP 3000X HR was used for analyzing the unaged material, as well as the material aged for 5 min and 100 h. All acquisitions were performed at a set temperature of 70 K using a pulse fraction of 20% of the DC voltage and a pulse frequency of 200 kHz. The specimens were prepared by standard electropolishing methods [11].

### **3. Results**

#### **3.1 Solution treated material**

The dense distribution of lath boundaries provides a high success rate in finding them by LEAP analysis, and in the aged conditions almost half of the analyses contain a boundary, see below. However, in the solution treated material lath boundaries could not be identified in the five analyses performed. It is therefore concluded that there is no significant enrichment at lath boundaries in this condition, as some boundaries must have been analyzed without being noticed. Also the matrix of the solution treated material does not contain any precipitates or clusters, and the elements are randomly distributed [5, 8].

### **3.2 Aging at 475°C for 5 minutes**

After 5 min aging, segregation of Mo, Si and P to lath boundaries could be observed. The amount of segregation is listed in Table 1, expressed as the excess number of ions per lath boundary area (Gibbs interfacial excess). The concentration profile of Mo measured perpendicular to the boundary is shown in Figure 1. The clear enrichment of Mo already after 5 min is somewhat surprising. From the depletion near the lath boundary, a diffusion constant of approximately  $2 \times 10^{-20}$  m<sup>2</sup>/s can be estimated, which is about two orders of magnitude larger than bulk diffusion of Mo in  $\alpha$ -Fe (or about the same as the diffusion constant at 590°C) [12]. The fast diffusion must be a result of the large degree of deformation and the high dislocation density.

Inside the laths, clustering of Cu, Ni, Ti, Al and Si has previously been reported in this condition [5, 8, 13]. The distributions of Mo, Si, Ti and Cu at and around the lath boundaries are shown in the reconstruction in Figure 2. It can be seen that the clusters are somewhat larger at the lath boundary, having a diameter approaching 2 nm as compared to about 1 nm in the matrix. The area number density of clusters at lath boundaries (number of clusters per lath boundary unit area) is presented in Table 2. The value was obtained by manually counting the number of clusters present at the lath boundaries, and the number was divided by the total size of the lath boundary area, obtained from the 3D reconstructions.

### **3.3 Aging at 475°C for 4 hours**

After 4 h, the former clusters in the matrix have developed into precipitates. The precipitates are in fact co-precipitates consisting of one Cu-rich 9R and one Ni<sub>3</sub>X precipitate. Roughly half of the Ni<sub>3</sub>X precipitates contain Si (about 3 at.%) and they are probably  $\gamma'$ -Ni<sub>3</sub>(Ti, Al, Si), whereas the

rest are free of Si and are probably  $\eta$ -Ni<sub>3</sub>(Ti, Al) [8]. At the lath boundaries, though, only 9R and  $\eta$  precipitates are present, also here as co-precipitates. The compositions of the lath boundary precipitates are presented in Table 3, and they are very similar to the compositions of the corresponding matrix precipitates [8]. The size of the lath boundary 9R precipitates is around 2 nm, and the  $\eta$  precipitates are elongated with a length about 7 nm. The lath boundary precipitates are only slightly larger than the precipitates in the matrix, but the density of precipitates is significantly higher, as seen in the reconstruction presented in Figure 3. The area number density of the co-precipitates is given in Table 2. The amount of segregation of Mo, Si and P has increased, see Table 1 and Figure 1.

### **3.4 Aging at 475°C for 40 hours**

After aging for 40 h, the precipitates in the matrix and at the lath boundaries have coarsened, see the reconstruction in Figure 4. Also the amount of segregation has increased, see Table 1 and Figure 1. The size of the elongated  $\eta$  precipitates is about 10 nm and also the 9R have grown to about 3 nm, at the same time as the area number density has decreased by a factor of three (see Table 2). As after 4 h of aging, the composition of the lath boundary precipitates, see Table 3, is very similar to the composition of the matrix precipitates [5, 8], and the size is marginally larger. In addition to the phases present after 4 h, Cr-rich  $\alpha'$  precipitates are present in the matrix after 40 h, in contact with  $\eta$  precipitates [8]. The  $\alpha'$  precipitates are, however, not located at the lath boundaries.

At the position of lath boundary precipitates, i.e. the  $\eta$  and 9R co-precipitates, there is no segregation of Mo, Si and P. Consequently, the film of the segregating species does not cover the entire lath boundary area, so there are holes in the film where the lath boundary precipitates

reside. This is illustrated in Figure 5, where the distribution of Ti and Cu, together with an iso-concentration surface of Mo+Si (>5at.%), is presented.

### **3.5 Aging at 475°C for 100 hours**

After 100 h a few significant changes have occurred to the microstructure, both in the matrix and at the lath boundaries [8]. First of all, rather large Mo-rich precipitates (>10 nm) have formed in the matrix. These are most likely the quasicrystalline R' phase, identified by Liu et al. using electron diffraction [14]. Also, the  $\gamma'$  precipitates have been replaced by G phase precipitates ( $\text{Ni}_{16}\text{Si}_7\text{Ti}_6$ ), with much higher Si content and lower Al content. Like the  $\gamma'$  phase, the G phase is not present at lath boundaries. The amount of Mo and Si at the lath boundaries is now much higher than after 40 h, and the segregation has turned into a precipitate film, about 5 nm thick, see Figure 6. The main composition, 36Fe-33Mo-15Cr-9Ni-5Si (at.%), is very similar to the composition of the R' precipitates in the matrix [8]. It is therefore suggested that the Mo-rich film, also observed by Hättestrand et al. [5], constitutes the quasicrystalline R' phase. The R' phase (both the lath boundary film and the matrix precipitates) also contains an elevated amount of trace elements (0.27C-0.10P-0.05B at.%). The precipitate film contains holes, where  $\eta$  and  $\gamma$  co-precipitates are located, see Figure 7. The film encompasses the co-precipitates in the lath boundary plane, but the film does not grow around the co-precipitates into the matrix. The  $\eta$  and  $\gamma$  phases at the lath boundaries have continued to coarsen and the size is now about 5 and 15 nm, respectively. Their composition is presented in Table 3.

## **4. Discussion**

The evolution of the microstructure of Nanoflex during aging at 475°C is intriguing, in particular the sudden appearance of Mo-rich R' phase both inside the matrix and at the lath boundaries.

This was recently explained in the following way [8]; at the early stages of aging, Si enters the  $\gamma'$  phase, which eventually transforms to G phase. Even though the Si content is much higher in the G phase than in the  $\gamma'$  phase, the volume fraction decreases substantially, and therefore Si becomes available for R' precipitation. Also at the lath boundaries the formation of R' phase is delayed. There is Mo and Si at the boundaries already after 5 min, and the amount increases slowly until 40 h. When the aging is extended to 100 h, the amount of Si and Mo increases by a factor of around 6 and 11, respectively, as compared to the amount present after 40 h. This clearly shows that the formation of the R' phase at the lath boundaries is not limited by the kinetics of segregation, but by the route of the precipitation sequence. This, in turn, must be governed by the interplay between the driving forces and the mobility of the many elements involved, in particular Si, Al and Ti seem to be important. The behavior of Si is noteworthy. At the early stages of aging it is incorporated in  $\gamma'$ -Ni<sub>3</sub>X and at the same time it segregates to the lath boundaries, but it is not incorporated in the precipitates there. After 4 h, the Si concentration in the matrix has reached 0.08 at.%, which remains constant until at least 100 h [8]. This means that the increase of Si at the lath boundaries after 40 h, compared to after 4 h, must come from Si leaving the coarsening  $\gamma'$ -Ni<sub>3</sub>X.

During aging of Nanoflex at 475°C coarsening of 9R and  $\eta$  starts long before 40 h [5, 8]. The (volume) number density of matrix 9R precipitates decreases as 1:0.37:0.14, for aging times of 4 h, 40 h and 100 h, respectively. For matrix  $\eta$  precipitates the corresponding values are 1:0.28:0.13. These values are rather similar to the values measured here for the area number density of lath boundary co-precipitates, which decreases as 1:0.36:0.21. This indicates that the coarsening kinetics of the lath boundary precipitates is similar to the coarsening kinetics of the matrix precipitates. Also, the lath boundary precipitates are only slightly larger than the matrix

precipitates. It seems likely that the segregation of Mo and Si and the subsequent formation of R' film at the lath boundaries limit the growth of 9R and  $\eta$  at the lath boundaries. In the absence of segregation and the R' film, faster growth would be expected at lath boundaries.

Although diffraction evidence is missing, the Mo-rich phase observed at the lath boundary is very likely the quasicrystalline R' phase, which definitely is present in the matrix after extended aging. The fact that the phase is present as a thin film (about 5 nm in thickness) means that the phase has a very low surface energy, which is a general feature of quasicrystals [15]. It is possible that the R' phase is present at the lath boundaries already after 40 h of aging, but the amount of segregation corresponds to less than one monolayer, so it is hardly relevant to discuss phase identity. The R' film present at the lath boundaries probably has a rather significant influence on the mechanical properties of the steel, and we believe that it is one of the reasons why the strength continues to increase for aging times substantially exceeding the onset of coarsening of the matrix and the lath boundary precipitates. Interestingly, the presence of a 1.5 nm thick precipitate film in a Mo bicrystal was found to increase the fracture strength by 30% (or 150 MPa) [16]. Also the toughness of Nanoflex is probably affected by the presence of the R' film, but no such measurements seem to have been published.

As in many APT studies of lath or grain boundaries, the limited amount of boundaries investigated calls for some caution in drawing precise conclusions. In the present investigation a total of ten lath boundaries have been analyzed, divided among four aging conditions. Together with previous work, where the matrix was thoroughly studied, and the consistency between matrix and lath boundary evolution, the amount of data should be sufficient to draw general conclusions, e.g. about which phases that are present at the lath boundaries. Regarding both area

number density and amount of segregation the accuracy is unfortunately not very high, as probably a large number of lath boundaries must be analyzed to account for variations. The compositions of lath boundary precipitates given in Table 3 are also somewhat uncertain. The Cu-rich 9R precipitates have a low evaporation field, leading to some spillover from neighboring matrix and  $\eta$  precipitates. The compositions were obtained using iso-concentration surfaces, and the threshold value chosen affects the result, as the precipitates are small.

## 5. Conclusions

During aging of the investigated steel at 475°C, Cu-rich 9R and  $\eta$ -Ni<sub>3</sub>(Ti, Al) precipitates form, in contact with each other, both inside laths and at lath boundaries, whereas  $\gamma'$ -Ni<sub>3</sub>(Ti, Al, Si), G phase and Cr-rich  $\alpha'$  only form inside the laths. The amount of segregation of Mo, Si and P to the lath boundaries increases with aging time, and after 100 h a ~5 nm thick quasicrystalline R' film is observed. The film does not cover the entire lath boundary area, but contains holes where  $\eta$ -Ni<sub>3</sub>(Ti, Al) and 9R co-precipitates penetrate through the film. The coarsening rate of the lath boundary co-precipitates is suppressed by segregation and the formation of the R' film.

## References

- [1]. J. Millan, D. Ponge, D. Raabe, P. Choi, O. Dimitrieva, Characterization of nano-sized precipitates in a Mn-based lean maraging steel by atom probe tomography, *Steel Res.* 82 (2011) 137-145.
- [2]. R. Schnitzer, M. Schober, S. Zinner, H. Leitner, Effect of Cu on the evolution of precipitation in an Fe-Cr-Ni-Al-Ti maraging steel, *Acta Mater.* 58 (2010) 3733-3741.
- [3]. H. Leitner, M. Schober, R. Schnitzer, Splitting phenomenon in the precipitation evolution in an Fe-Ni-Al-Ti-Cr stainless steel, *Acta Mater.* 58 (2010) 1261-1269.
- [4]. D.H. Ping, M. Ohnuma, Y. Hirakawa, Y. Kadoya, K. Hono, Microstructural evolution in 13Cr-8Ni-2.5Mo-2Al martensitic precipitation-hardened stainless steel, *Mater. Sci. Eng. A394* (2005) 285-295.
- [5]. M. Hattestrand, J.-O. Nilsson, K. Stiller, P. Liu, M. Andersson, Precipitation hardening in a 12%Cr-9%Ni-4%Mo-2%Cu stainless steel, *Acta Mater.* 52 (2004) 1023-1037.
- [6]. P. Liu, A. Hultin Stigenberg, J.-O. Nilsson, Isothermally formed quasicrystalline precipitates used for strengthening in a new maraging stainless steel, *Scr. Metall.* 31(1994) 249-254.
- [7]. J.-O. Nilsson, A. Hultin Stigenberg, P. Liu, Isothermal formation of quasicrystalline precipitates and their effect on strength in a 12Cr-9Ni-4Mo maraging stainless steel, *Metall. Trans. A* 25A (1994) 2225-2233.
- [8]. M. Thuvander, M. Andersson, K. Stiller, Precipitation process of martensitic PH stainless steel Nanoflex, *Mater. Sci. Technol.* 28 (2012) 695-701.
- [9]. K. Stiller, H.-O. Andrén, M. Andersson, Precipitation in maraging and martensitic chromium steels – what can we learn using 3-DAP and EFTEM, *Mater. Sci. Technol.* 24 (2008) 633-640.
- [10]. T.F. Kelly, D.J. Larson, Local electrode atom probes, *Mater. Charact.* 44 (2000) 59-85.

- [11]. M.K. Miller, A. Cerezo, M.G. Hetherington, G.D.W. Smith, Atom probe field ion microscopy, Oxford University Press, Oxford, 1996.
- [12]. H. Nitta, T. Yamamoto, R. Kanno, K. Takasawa, T. Iida, Y. Yamazaki, S. Ogu, Y. Iijima, Self-diffusion in iron-based Fe-Mo alloys, *Acta Mater.* 50 (2002) 4117-4125.
- [13]. K. Stiller, M. Hattestrand, F. Danoix, Precipitation in 9Ni-12Cr-2Cu maraging steels, *Acta Mater.* 46 (1998) 6063-6073.
- [14]. P. Liu, A.H. Stigenberg, J.-O. Nilsson, Quasicrystalline and crystalline precipitation during isothermal tempering in a 12Cr-9Ni-4Mo maraging stainless steel, *Acta Metall. Mater.* 43 (1995) 2881-2890.
- [15]. E. Huttunen-Saarivirta, Microstructure, fabrication and properties of quasicrystalline Al-Cu-Fe alloys: a review, *J. Alloys Comp.* 363 (2004) 150-174.
- [16]. M. Bacia, J.M. Pénisson, M. Biscondi, Carbon precipitation in a  $\Sigma=5$  tilt boundary in molybdenum, *Mater. Sci. Forum* 207-209 (1996) 193-196.

## Tables

Table 1. Interfacial excess ( $\text{nm}^{-2}$ ) measured at lath boundaries.

Aging Time	5 min	4 h	40 h	100 h
Mo	$1.2 \pm 0.5$	$2.0 \pm 0.5$	$8.3 \pm 2$	$93 \pm 20$
Si	$0.32 \pm 0.15$	$0.73 \pm 0.3$	$2.1 \pm 0.5$	$12 \pm 4$
P	$0.10 \pm 0.05$	$0.10 \pm 0.05$	$0.09 \pm 0.5$	$0.28 \pm 0.15$

Table 2. Area number density of Cu-rich 9R and  $\eta\text{-Ni}_3(\text{Ti, Al})$  co-precipitates at lath boundaries ( $10^{15} \text{ m}^{-2}$ ).

Aging Time	5 min	4 h	40 h	100 h
Area Number Density	$9 \pm 2$	$14 \pm 2$	$5 \pm 1$	$3 \pm 1$

Table 3. Composition (at.%) of 9R and  $\eta\text{-Ni}_3(\text{Ti, Al})$  precipitates at lath boundaries.

Phase	9R			$\eta\text{-Ni}_3(\text{Ti, Al})$		
	4 h	40 h	100 h	4 h	40 h	100 h
Cu	$61.5 \pm 1.9$	$65.2 \pm 0.6$	$72.5 \pm 0.8$	$2.0 \pm 0.4$	$2.5 \pm 0.1$	$2.8 \pm 0.2$
Ni	$9.0 \pm 0.7$	$11.4 \pm 0.2$	$12.0 \pm 0.7$	$63.0 \pm 1.0$	$65.8 \pm 0.3$	$66.5 \pm 0.7$
Ti	$1.2 \pm 0.4$	$1.1 \pm 0.1$	$1.0 \pm 0.1$	$17.6 \pm 0.7$	$16.8 \pm 0.3$	$15.8 \pm 0.8$
Al	$2.1 \pm 0.7$	$2.0 \pm 0.1$	$1.3 \pm 0.2$	$5.7 \pm 0.3$	$7.4 \pm 0.1$	$6.3 \pm 0.4$
Fe	$17.0 \pm 1.0$	$12.6 \pm 0.3$	$7.4 \pm 0.5$	$7.8 \pm 0.6$	$3.4 \pm 0.1$	$3.6 \pm 0.2$
Mo	$6.0 \pm 1.6$	$5.2 \pm 0.7$	$2.5 \pm 0.3$	$2.0 \pm 0.3$	$2.4 \pm 0.1$	$2.5 \pm 0.4$
Cr	$2.1 \pm 0.3$	$1.9 \pm 0.2$	$1.8 \pm 0.2$	$1.1 \pm 0.2$	$0.93 \pm 0.05$	$1.2 \pm 0.1$
Si	-	$0.04 \pm 0.03$	$0.41 \pm 0.11$	$0.16 \pm 0.06$	$0.20 \pm 0.02$	$0.23 \pm 0.09$
Mn	$0.93 \pm 0.30$	$0.64 \pm 0.08$	$1.1 \pm 0.2$	$0.58 \pm 0.09$	$0.41 \pm 0.02$	$0.85 \pm 0.10$

## Figure captions

Figure 1. Concentration profiles of Mo measured perpendicular to the lath boundary plane for different aging times at 475°C, maraging stainless steel Nanoflex.

Figure 2. Elemental distribution at a lath boundary in maraging stainless steel Nanoflex aged for 5 min at 475°C. The box size is 30×30×60 nm<sup>3</sup>.

Figure 3. Elemental distribution at a lath boundary in maraging stainless steel Nanoflex aged for 4 h at 475°C. The box size is 25×25×50 nm<sup>3</sup>.

Figure 4. Elemental distribution at a lath boundary in maraging stainless steel Nanoflex aged for 40 h at 475°C. The box size is 40×40×80 nm<sup>3</sup>.

Figure 5. Lath boundary in maraging stainless steel Nanoflex aged for 40 h at 475°C viewed perpendicular to the boundary plane. The iso-concentration surface was made for a threshold of Mo+Si of 5 at.%.

Figure 6. Elemental distribution at a lath boundary in maraging stainless steel Nanoflex aged for 100 h at 475°C. The box size is 40×40×40 nm<sup>3</sup>.

Figure 7. Precipitation at a lath boundary in the maraging stainless steel Nanoflex aged for 100 h at 475°C. The Mo-rich R' phase (purple iso-concentration surface) forms a holey film with elongated η (blue iso-concentration surface) and 9R (red iso-concentration surface) precipitates

located at the holes. The box size is  $80 \times 80 \times 55 \text{ nm}^3$ . For clarity, precipitates not located at the lath boundary are not shown. The iso-concentration surfaces were made for thresholds of 15 at.% Mo+Si, 70 at.% Ni+Al+Ti and 60 at.% Cu, respectively.

Figure 1.

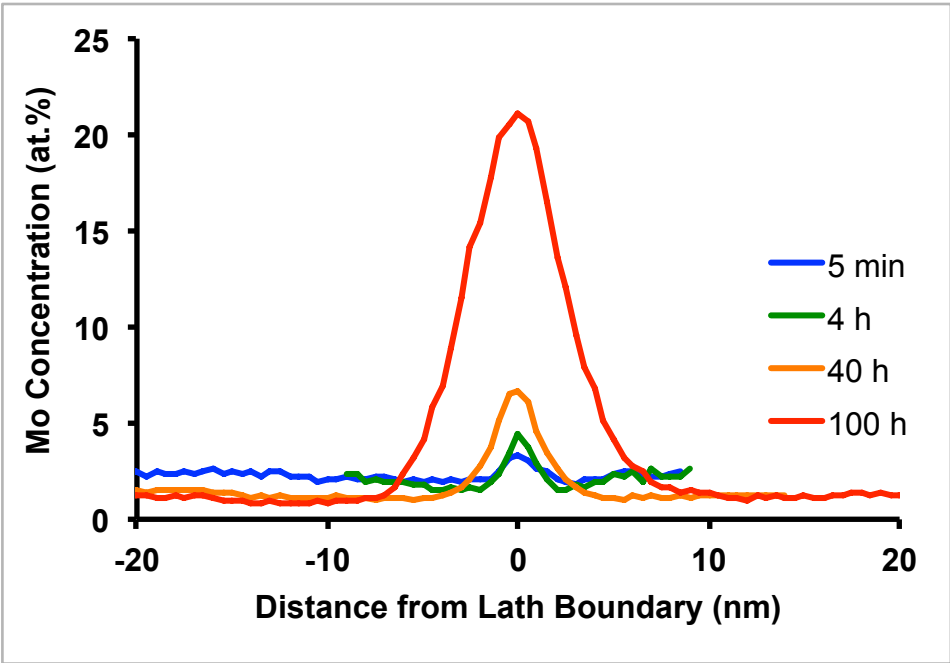


Figure 2.

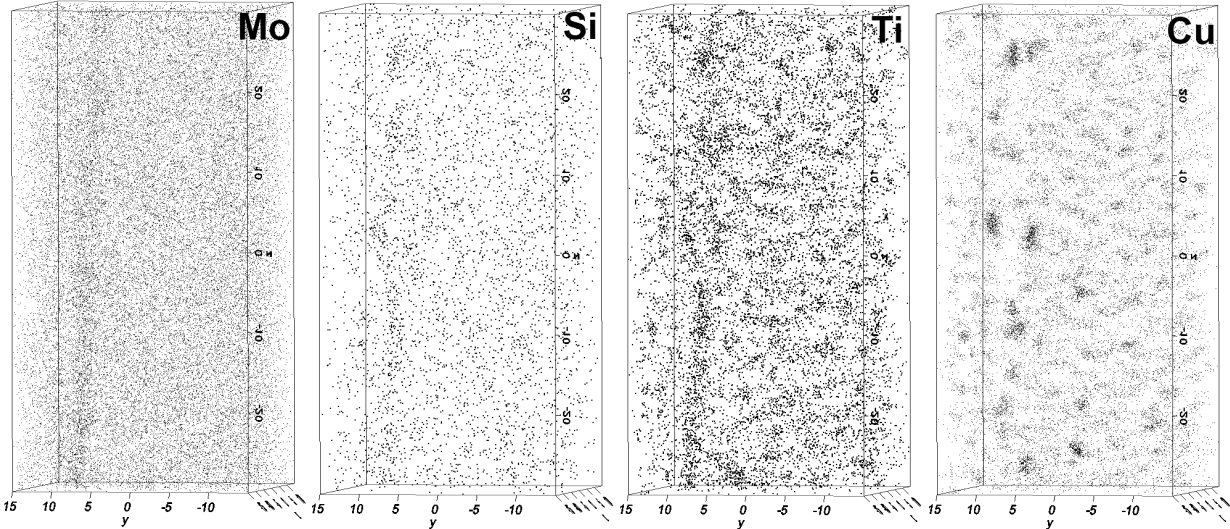


Figure 3.

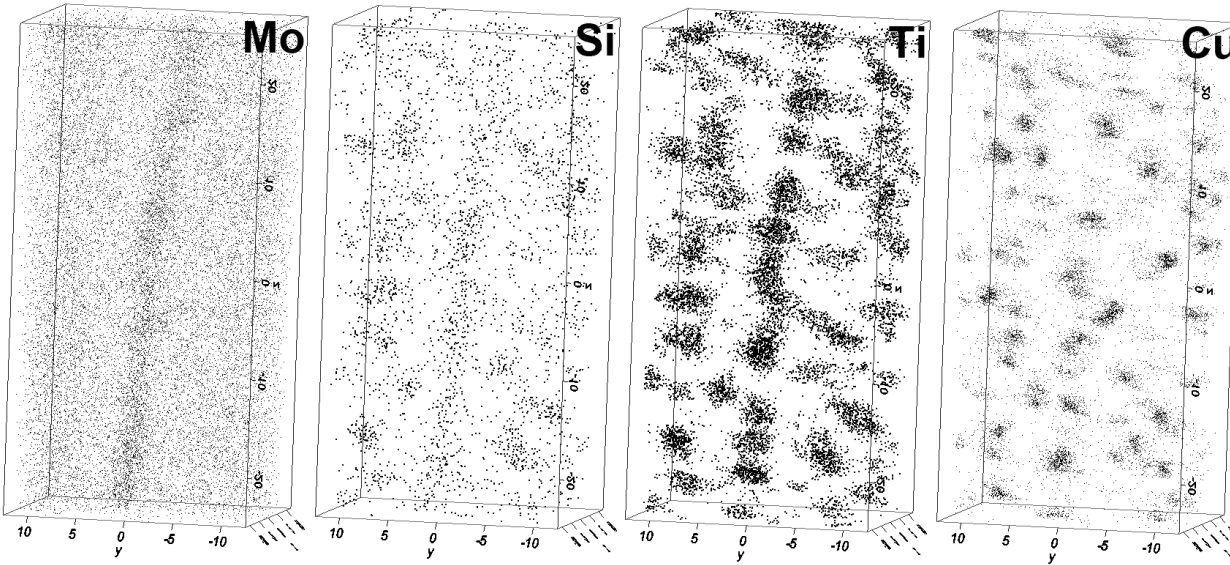


Figure 4.

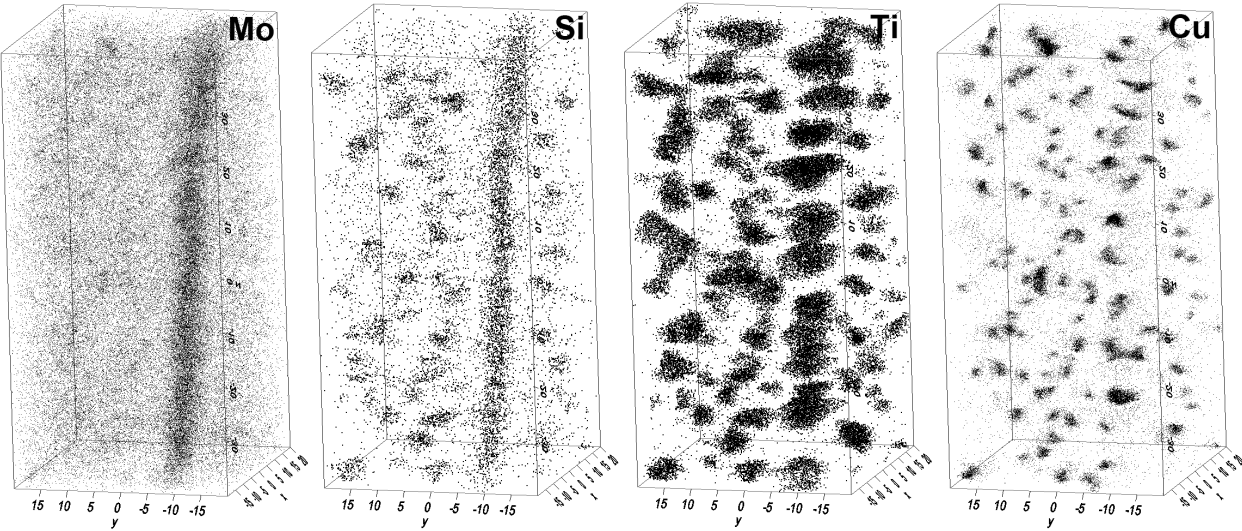


Figure 5.

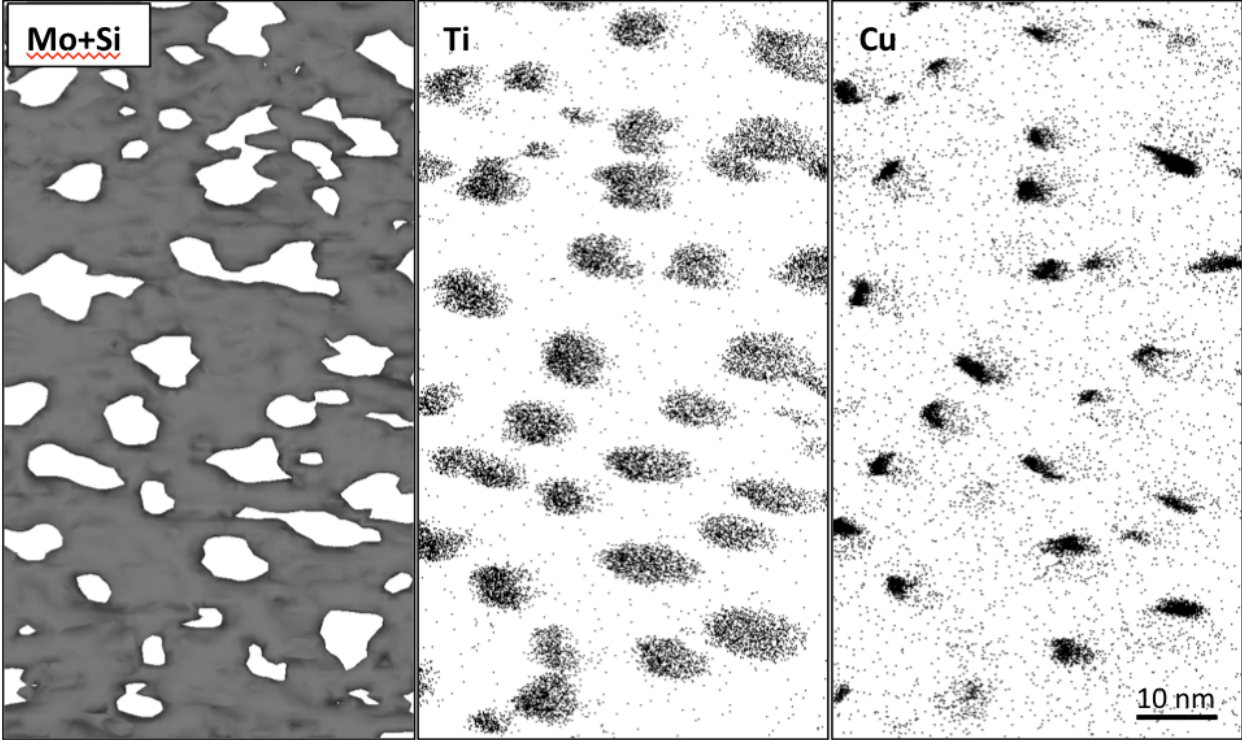


Figure 6.

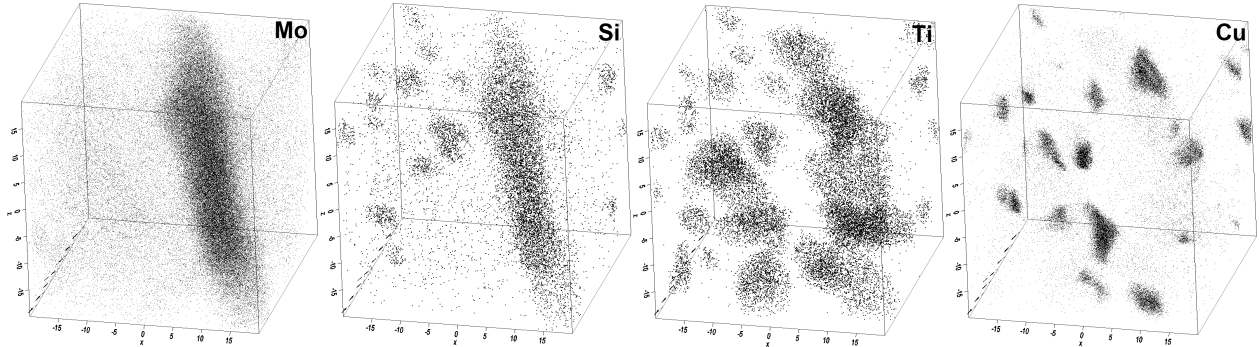


Figure 7.

